The positive radiative forcing by the substantial SO₂ emission reductions is counteracted by decreased BC concentrations in China over the recent decade

Mingxu Liu[1] and Hitoshi Matsui[1]

[1]Graduate School of Environmental Studies, Nagoya University, Nagoya, Japan

Corresponding to: Hitoshi Matsui (matsui@nagoya-u.jp)

Abstract. Anthropogenic emissions in China play an important role in altering global radiation budget. Over the recent decade, the clean-air options in China result in substantial reductions in anthropogenic emissions, especially sulfur dioxide (SO₂), and improved air quality. However, the associated changes in aerosol climate effects are poorly understood. In this study, we use an advanced global climate model integrated with latest anthropogenic emission inventory to estimate the changes in the aerosol radiative forcings by the emission variation in China between 2008 and 2016. First, our simulations exhibit decreases of 46% and 25% for the annual mean surface-level sulfate and black carbon (BC) mass concentrations in East China, respectively, which is the key region subject to stringent emission control options. The decreasing tendency of aerosol optical depth and aerosol absorption optical depth retrieved by satellites is also captured by the model for the period. We find that the resultant net radiative forcing by the changes in the BC and SO₂ emissions is −0.04 W m⁻² in East China. The substantial reductions in SO₂ emissions diminish the scattering effects of sulfate and lead to an overall change of +0.17 W m⁻² for the annual mean all-sky shortwave aerosol direct radiative forcing at the top of the atmosphere and +0.13 W m⁻² for aerosol-induced cloud radiative forcing. In the meantime, the reduction in BC emissions induces a negative BC radiative forcing of −0.34 W m⁻². By accounting for the joint effect of BC and SO₂ emissions, our results demonstrate that the positive radiative forcing by the SO₂ emission reductions is counteracted by the decrease of BC in China over the recent decade. While the local radiative forcing is small due to the counteracted effects of SO₂ and BC emissions, it is relatively larger (+0.16 W m⁻²) over the north Pacific remote regions for this period, primarily contributed by the reductions in sulfate particles and their effects on cloud properties. With a comprehensive future emission scenario for 2030 and 2050 developed by the recent study, we predict that the strictest environmental policies will induce the change of aerosol radiative forcings of +0.55 and +1.23 W m⁻² over East China between 2016−2030 and 2016−2050, respectively. Targeted emission control policies are desirable to improve air quality and mitigate climate change in the future.

1. Introduction

Aerosols perturb the global energy balance by aerosol-radiation interactions, such as the scattering and absorption of sunlight (Charlson et al., 1992), and by aerosol-cloud interactions through the activation of cloud condensation nuclei (CCN) particles

30 into cloud droplets, which impact on both the cloud albedo and lifetime (Twomey, 1974; Andreae and Rosenfeld, 2008). The changes in anthropogenic aerosol concentrations from preindustrial to present days are estimated to induce a global-mean net cooling effect of −0.4 to −1.5 W m^{-2} at the top of the atmosphere (TOA) that partly mask the warming effects by increased carbon dioxide (Boucher et al., 2013).

It is commonly known that black carbon (BC) and sulfate aerosols are important contributors to the radiation absorption and
35 scattering effects of anthropogenic aerosols in the global scale. Bond et al. (2013) estimated that the industrial-era (1750−2015) direct radiative forcing of BC is 0.71 W m^{-2}. Until now, uncertainties embedded in the radiative forcing of BC are still large due to the insufficient treatment of BC atmospheric processes in climate models including the impacts of BC on liquid clouds (Koch and Del Genio, 2010; Chung and Seinfeld, 2002) and the role of BC in acting as ice nuclei (Kulkarni et al., 2016). Moreover, the mixing state is one of the key parameters that determine the optical properties and CCN activity of BC (Jacobson,
40 2001; Stier et al., 2006; Matsui, 2016). Recent studies find that explicit representation of BC aging processes can increase the confidence in the estimates of BC direct radiation forcing (Matsui et al., 2018). Unlike BC that is directly emitted into the atmosphere, sulfate aerosols mainly originate from the chemical transform of sulfur dioxide (SO$_2$) via the photochemical oxidation by OH radical, aqueous and heterogeneous reactions (Seinfeld and Pandis, 2016). The accurate estimate of sulfate radiative forcing relies heavily on the representation of secondary sulfate formation in climate models and SO$_2$ emissions
45 (Huang et al., 2015). Sulfate aerosols are estimated to exert a global-mean direct radiative forcing of −0.32 W m^{-2} for the time period of 1750 to 2010 (Myhre et al., 2013), with remarkable radiative perturbation in the north mid-latitude region (20 °–40 ° N) due to the rapidly increased anthropogenic SO$_2$ emissions in China over the past few decades. The tremendous anthropogenic emissions in China not only result in severe air pollution, but also significantly alter the global aerosol radiation budget (Li et al., 2016).

50 During the past ten years, China has implemented stringent air pollution control measures and the SO$_2$ emissions started to decrease in 2007 with the application of flue gas desulfurization in the power sector. Especially since 2013, the toughest-ever clean air policies have led to substantial reductions in anthropogenic emissions in China. According to the latest emission inventory, the national annual emissions of SO$_2$, NO$_x$, BC, and organic carbon (OC) have declined by 62%, 17%, 27%, and 35%, respectively during 2010−2017 (Zheng et al., 2018). Recent studies have demonstrated significant improvements of air
55 quality in China attributable to those various emission control measures (Zhang et al., 2019). Specifically, SO$_2$ emissions exhibited the most notable reduction among all pollutants for this period, which reduce the concentrations of sulfate aerosols dramatically and mitigate the PM$_{2.5}$ pollution and acid rain issues (Liu et al., 2020; Liu et al., 2018). However, few studies have reported how those substantial changes in anthropogenic components impact radiation energy budget in China and surrounding areas. Paulot et al. (2018) estimate the changes in the aerosol radiative effects in eastern China from 2001 to 2015,
60 but the results may be not realistic since they adopt the clear-sky condition and external mixing for aerosols in their simulations and don't consider the aerosol-cloud interaction, all of which are important in the calculation of aerosol total radiative effects (Ghan, 2013).

In this study, we aim to evaluate the response of aerosol radiative forcings (RF) including both direct radiative effects and aerosol effects on clouds to the change in anthropogenic emissions in China between 2008 and 2016. An advanced global climate model integrated with the latest bottom-up emission inventory for China is used to diagnose the changes in RF from different aerosol components (sulfate, nitrate, BC etc.) over the recent decade. Furthermore, we perform another experiment to predict the radiative effects of aerosols with projected emission scenarios for the years of 2030 and 2050. Our results can provide implications for understanding the aerosol effects on climate in the future.

2. Methods

2.1 Model experiments

In this study, we use the Community Atmospheric Model version 5 (CAM5) with the Aerosol Two-dimensional bin module for foRmation and Aging Simulation version 2 (CAM5/ATRAS2) (Matsui and Mahowald, 2017; Matsui, 2017). The release version of CAM5 can simulation emission, gas-phase chemistry (MOZART), aerosol microphysical and secondary formation processes, wet/dry deposition, and aerosol-radiation-cloud interactions (Liu et al., 2012). The ATRAS2 module (Matsui et al., 2014) uses a two-dimensional sectional representation with 12 particle size bins (from 1 to 10000 nm in diameter) and 8 BC mixing state bins (from fresh BC to aged BC-containing particles) for various microphysical and chemical processes of aerosols, including new particle formation, condensation/coagulation, aerosol activation, wet/dry deposition, and interactions with radiation and clouds. The model treats aerosol–cloud interactions in stratiform clouds using a physically based two-moment parameterization that considers the aerosol effects on cloud properties (Morrison and Gettelman, 2008). The secondary formation of sulfate is found to be important when simulation sulfate concentrations in China, but is not represented well in current chemistry-climate models (Hung and Hoffmann, 2015; Cheng et al., 2016). To better reproduce the temporal evolution of sulfate concentrations in China, we add a new pathway suggested by previous studies for secondary sulfate formation in our model, that is, the heterogeneous oxidation of gaseous SO_2 to particulate sulfate onto aerosol surfaces under high humidity conditions (Huang et al., 2014). The uptake coefficients of SO_2 are specified as the range between 2.0×10^{-5} and 1.0×10^{-4} under the relative humidity of 50−100%.

The model is running at the horizontal resolution of $1.9°\times2.5°$ with 30 vertical layers from the surface to ~40 km on the global scale. Several simulation experiments are designed with different inputs of anthropogenic emissions as shown in Table 1. We vary the anthropogenic emissions of all species between 2008 and 2016 for China, termed as Exp08 and Exp16, respectively. The separate contributions of SO_2 and BC and their joint effects are identified with the cases of Exp16SO2, Exp16BC, and Exp16. The meteorological fields were nudged by using the Modern-Era Retrospective analysis for Research and Applications Version 2 (MERRA2) data and were fixed at 2008 to isolate the contribution of emissions on radiation effects. We perform 2-year simulations and the first year is for spin-up and the second year is for analysis.

We diagnose both the aerosol direct radiative effects (DRE) and aerosol effects on clouds (semi- and indirect effects, termed as cloud radiative effects, CRE) in the model. The changes in DRE and CRE between the emissions years of 2008 and 2016 can be regarded as aerosol RF (direct radiative forcing (DRF) and aerosol-induced cloud radiative forcing (CRF)) owing to the variation of anthropogenic emissions for this period. Here, the DRE at TOA for specific aerosol component is online calculated as the differences between the standard and the diagnosed radiative fluxes that subtracting this species in the radiation module. Then the aerosol DRF is calculated as the difference of DRE between 2008 and 2016. The aerosol effects on clouds are diagnosed following Ghan (2013) using the variables of clean-sky (neglecting the scattering and absorption of all aerosol species) radiative flux. The CRF calculated in this study is scaled by comparing our global model results during the industrial-era to the best estimate of effective radiative forcing due to aerosol-cloud interactions by the Fifth Assessment Report of the Intergovernmental Panel on Climate Change (IPCC AR5) (Boucher et al., 2013).

Table 1. Model simulation experiments with different emission scenarios for China

	SO₂	BC	Others
Exp08	2008	2008	2008
Exp16	2016	2016	2016
Exp16SO2	2016	2008	2008
Exp16BC	2008	2016	2008

2.2 Anthropogenic emissions for China

The global anthropogenic emissions for the year of 2008 are taken from Hoesly et al. (2018) based on the Community Emissions Data System, while the emissions in China are replaced by the Multi-resolution Emission Inventory (MEIC) for 2008 or 2016, which provide a more realistic representation of China's emissions from fossil fuels and biofuels (Zheng et al., 2018). In addition, the ammonia emissions in China are taken from Liu et al. (2018), in which the estimates of agricultural ammonia emissions are well constrained and show good performance in the simulation of atmospheric ammonia. As shown in Table 2, several major species including BC, organic aerosols (OA), and SO₂ experience reductions between 2008 and 2016 due to the clean-air policy in China in this period. The majority (more than 90%) of those emission reductions are found in East China (marked in Fig. 1), which is characterized with dense population and economic activities and is the key region subject to stringent air pollution control. For instance, emission reductions in East China are 57% for SO₂, 27% for BC, and 30% for OC.

Table 2. Anthropogenic emissions for major species in China and East China (EC) between 2008 and 2016 (units: Tg year[-1])

	2008		2016	
	China	EC	China	EC
BC	1.7	1.5	1.3	1.1
NO_x	24	21	23	19
OC	3.2	2.7	2.3	1.9
$PM_{2.5}$	12	11	8.1	6.9
SO_2	30	28	13	12

2.3 Observation data

In order to evaluate the model performance for aerosol simulations, we collect the monthly measurement concentrations of inorganic aerosol chemical components (sulfate, nitrate, and ammonium) from Acid Deposition Monitoring Network in East Asia (EANET). The EANET stations used in this study including one site in southern China and nine sites in western and central Japan. In addition, we use AERONET (Aerosol Robotic Network) surface stations which give high quality sunphotometer measurements of aerosol properties like aerosol optical depth (AOD) and single scatter albedo (SSA). The Beijing (39.98 °N, 116.38 °E) and Xianghe (39.75 °N, 116.96 °E) stations in AERONET have long-term data records and can be used to compare with our inter-annual simulations. The AOD retrieved by the Multi-angle Imaging Spectroradiometer (MISR) at 555 nm are used for comparison with our model results.

3. Results

3.1 Changes in the burdens of sulfate and BC mass

We first evaluate the simulated sulfate mass concentrations with the EANET observations in China and Japan between the years of 2008 and 2016 (Fig. 1a, b). The simulated sulfate using CAM5/ATRAS2 model agrees well with observations with respect to the magnitude and spatial patterns, showing high annual mean concentrations up to 20 µg m^{-3} in East China in 2008 and mostly decreasing to less than 10 µg m^{-3} in 2016 due to the reductions of about 60% in SO_2 emissions. The overall decrease of annual mean sulfate concentrations in East China is about 3.5 µg m^{-3} (46%) in our simulations, which is in agreement with the observations and air quality model results by recent studies for the same period (Liu et al., 2018). Higher reductions of more than 10 µg m^{-3} are found in northern part of East China (Figure 1a, b), where the SO_2 emission reductions are the most notable in the country (Li et al., 2017). In the meantime, the sulfate mass column burden (integral of concentrations from surface to the top of atmosphere) averaged over East China exhibits a decrease of 4.5 mg m^{-2}, equal to 35% of that burden in 2008 (Fig. 2a, c). Moreover, the averaged sulfate burden decreases by 0.38 mg m^{-2} (−18%) in the northern Pacific (the region marked in Fig. 2), reflecting the impacts of SO_2 emission reductions from East China to the downwind regions.

We verity the trend in modeled BC concentrations using the measurements in three typical sites located in East China and western Japan. The long-term observational records of BC concentrations in Beijing and Shanghai present clear decreasing trends over the recent decade (Xia et al., 2020; Wei et al., 2020). The annual mean surface BC decreases from 8.5 µg m^{-3} in 2008 to 3.5 µg m^{-3} in 2016 in Beijing, and from about 4.0 µg m^{-3} to 2.2 µg m^{-3} in Shanghai. Similar reductions are found in our simulations for the emission years of 2008 and 2016 (Fig. 1c, d), with the averaged decrease of 25% over East China. The model also captures the inter-annual decline in BC observed at Fukue Island in western Japan, which is attributed to the reduction of the BC emissions in East China (Kanaya et al., 2019). Moreover, annual mean BC burdens decrease by 0.38 mg m^{-2} for this region and by 0.016 mg m^{-2} in the northern Pacific (Fig. 2b). The column burdens of BC experience reductions of 22% in East China and 13% in the northern Pacific (Fig. 2d). In general, the results suggest that the integration of CAM5/ATRAS2 model and the MEIC emission inventory for China can reproduce the observed inter-annual trend in the sulfate and BC concentrations over the recent decade.
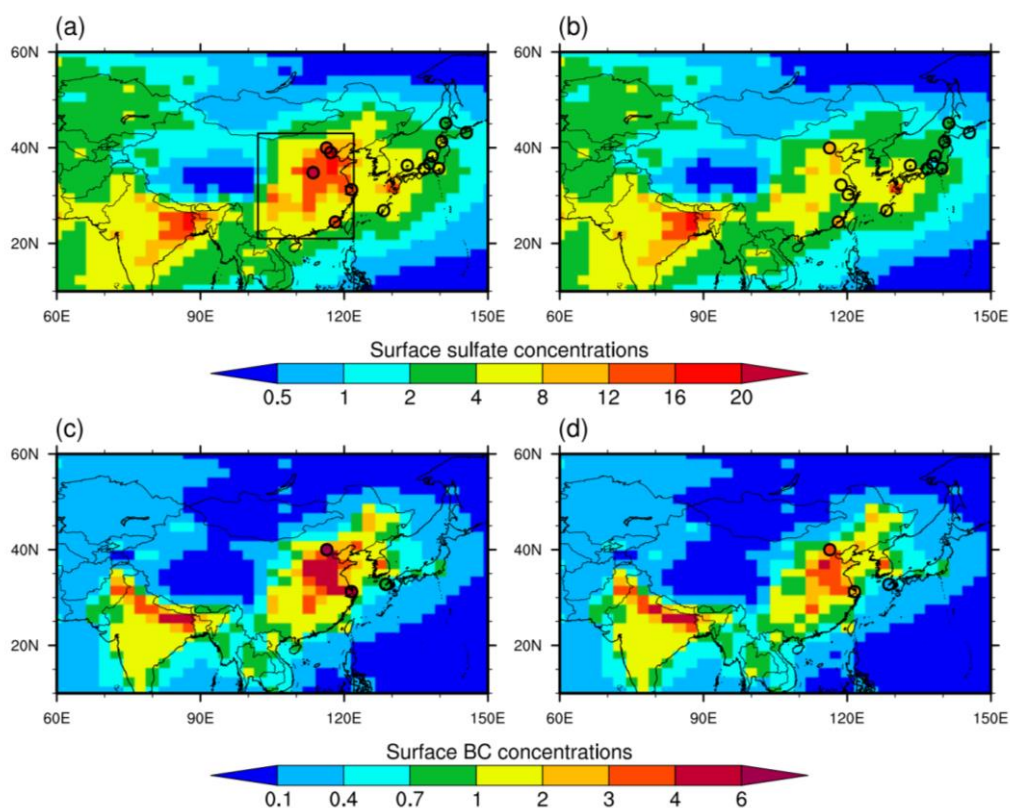
Figure 1. Map of simulated surface PM$_{2.5}$ sulfate (a-b) and BC (c-d) concentrations (units: µg m^{-3}) over China and surrounding areas between 2008 (left column) and 2016 (right column). The observations of the annual mean sulfate and BC concentrations obtained from EANET and literatures (Table S2) are shown for comparison. The geographical range of East China (21°−43° N, 102°−122° E) is marked in Fig. 1a.
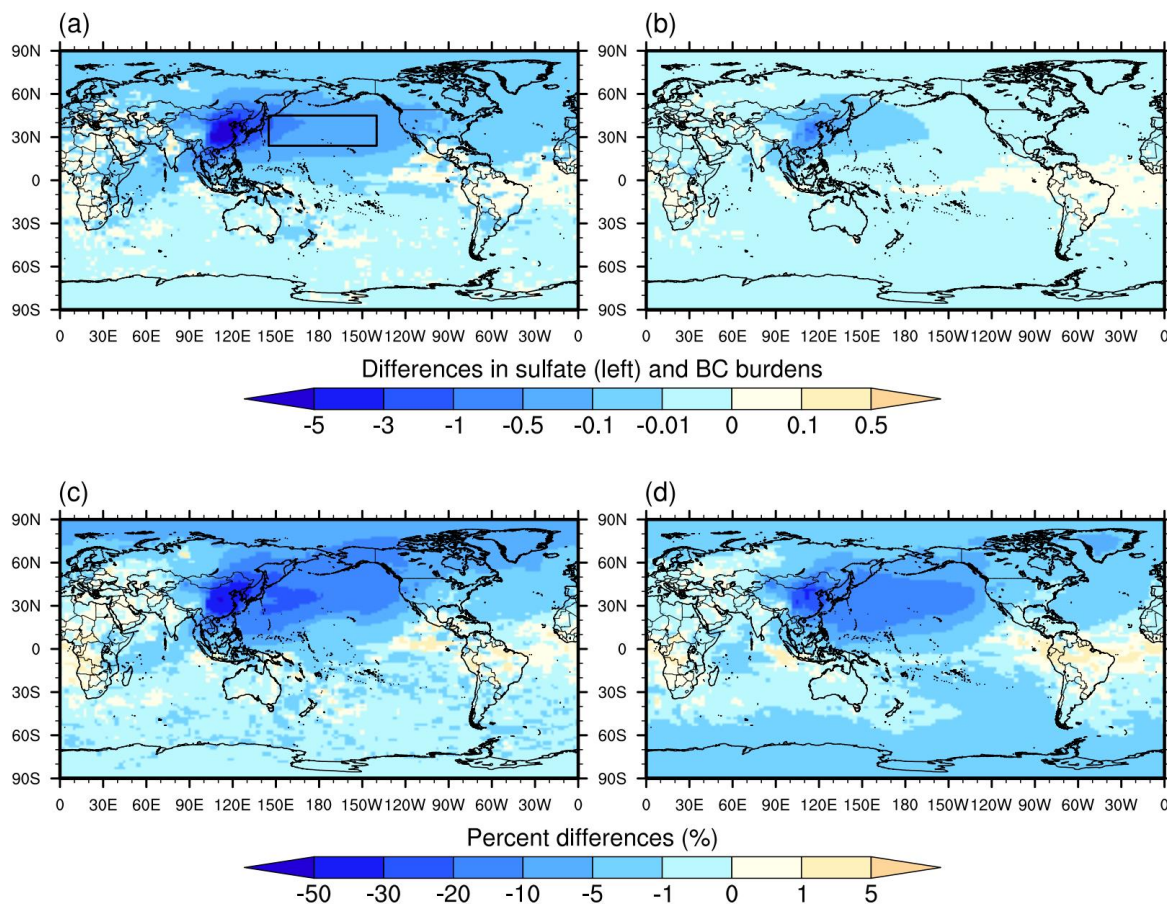
Figure 2. Change in particulate sulfate and BC burdens due to the emission variation in China between 2008 and 2016. (a-b) and (c-d) denote the mass (mg m^{-2}) and percent differences (%), respectively. The north Pacific region (24°−45° N, 145 ° E−140 °W) is marked with the black box in Fig. 2a

Our model shows similar concentrations (10−20 μg m^{-3}) of particulate nitrate with the measurements in several sites in northern parts of East China (Fig. S1). We find that the annual mean nitrate concentrations are elevated by about 1.0 μg m^{-3} (20%) in East China between 2008 and 2016, primarily resulting from the reductions of ammonium sulfate particles, which can release free ammonia to facilitate the formation of ammonium nitrate (Ansari and Pandis, 1998). Similar increase of nitrate in the region is reported by Liu et al. (2018) for the same period using a regional chemical transport model. In addition, the annual mean concentrations of particulate ammonium and organic aerosols in East China are reduced by 0.41 μg m^{-3} and 0.13 μg m^{-3}, respectively.

Furthermore, the reductions in sulfate and BC burdens would dampen new particle formation and the growth of particles via condensation and coagulation processes to serve as CCN. Figure 3 shows the longitude-height (pressure in hPa) distribution

of the changes (%) in particle number concentrations with the diameters larger than 10 nm (N10) and diagnostic CCN numbers at supersaturation of 0.4% (CCN0.4) along the latitude 35 °N, which is characterized with notable reductions in sulfate and BC burdens. The N10 shows decreases of about 20% in East China (100−130 °E) from the surface to 300 hPa. The simulated CCN0.4 concentrations decrease not only in East China (30%) but also in the middle troposphere (700−200 hPa) over the

175   north Pacific region (10%). According to the sensitivity experiment Exp16SO2, these variations in N10 and CCN0.4 are primarily accounted by decreases of particulate sulfate in East China and the downwind regions. The decreases of CCN concentrations would alter the cloud properties through the activation into cloud droplets and subsequently change the radiation budget, which is discussed in the next sections.
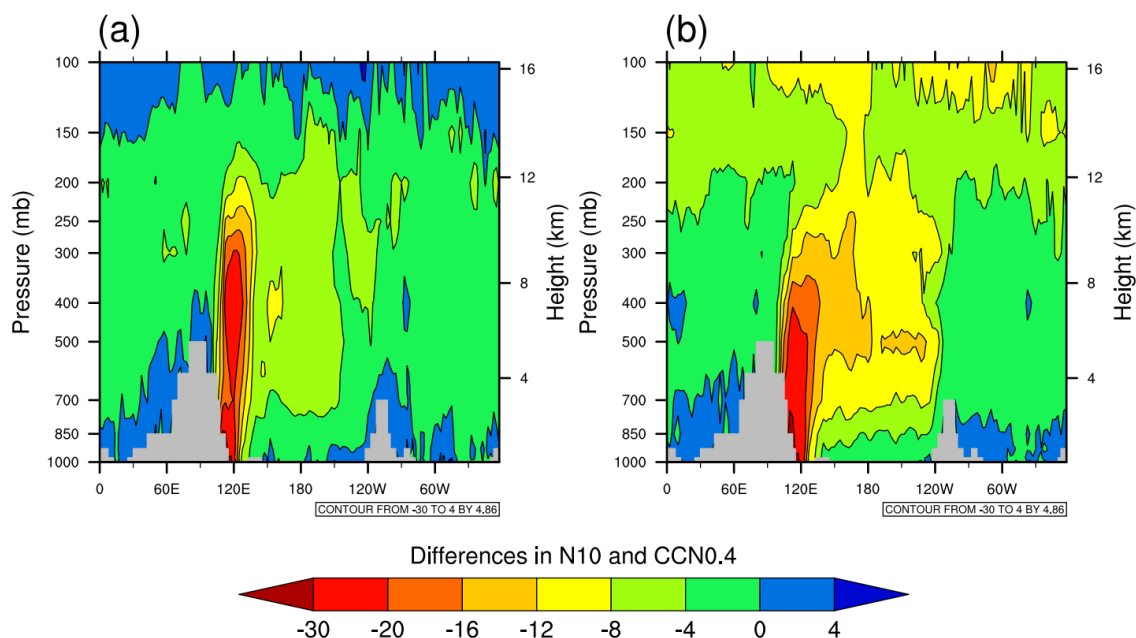
180   **Figure 3**. Pressure-longitude distribution of the annual-mean percent differences in the N10 and CCN0.4 along the latitude 35 °N due to the emission variation in China between 2008 and 2016

3.2 Trends in aerosol optical properties

The pronounced variations of sulfate and BC particles between 2008 and 2016 induce the change in aerosol optical properties, i.e., aerosol optical depth (AOD) and absorption aerosol optical depth (AAOD) at 550 nm. First, we find that our CAM model

185   can capture the observed hotspots of AOD (> 0.3) over North Africa, East China, the tropical Atlantic Ocean, and West-South Asia by comparing to the MISR measurements (Fig. S2). Specifically, the annual mean AOD for East China in the model (0.25) is lower than that from MISR (0.34) in the year of 2008. It should be pointed out that the negative bias of AOD values relative to the measurements are commonly found over East Asia by the CAM model (Sockol and Small Griswold, 2017; He et al., 2015). Figure 4 presents the differences of these optical variables at 550 nm between 2008 and 2016. Corresponding to

190 the reductions in sulfate and BC mass concentrations, AOD show percent decreases of 2−10% over most of East China (marked in black box in Fig. 4), on average of 5.2%, in which the variation in AOD from sulfate particles has a dominant contribution to the total. Recent studies find a statistically significant decrease of 10−20% for AOD in the same region over the recent decade based on the remote sensing observations from the surface (AERONET) and space (MODIS and MISR (Fig. S2)) (Li, 2020; Zhang et al., 2017; Zhao et al., 2017). The moderate underestimation of AOD trends may be related to the negative bias

195 of modeled AOD as abovementioned.

In the meantime, the simulated annual mean AAOD decreases by about 16% (from 0.018 to 0.015) over East China between the emission years of 2008 and 2016 (Fig. 4), with salient decrease up to 40% in the northern part, which is subject to high reductions of BC emissions and resultant column burdens (Fig. 2). We also compare the model results with the averaged observations in two AERONET stations (located in the same model grid and labelled in Fig. 4) with long-term records available.

200 The AAOD from AERONET are calculated using the observed AOD and SSA at 550 nm wavelength taken from the monthly Level 2 datasets. The annual mean observed AOD and AAOD decrease by about 29% and 40%, respectively, while our model underestimates such an observed trend of AOD at this local site, but agreed with AAOD.
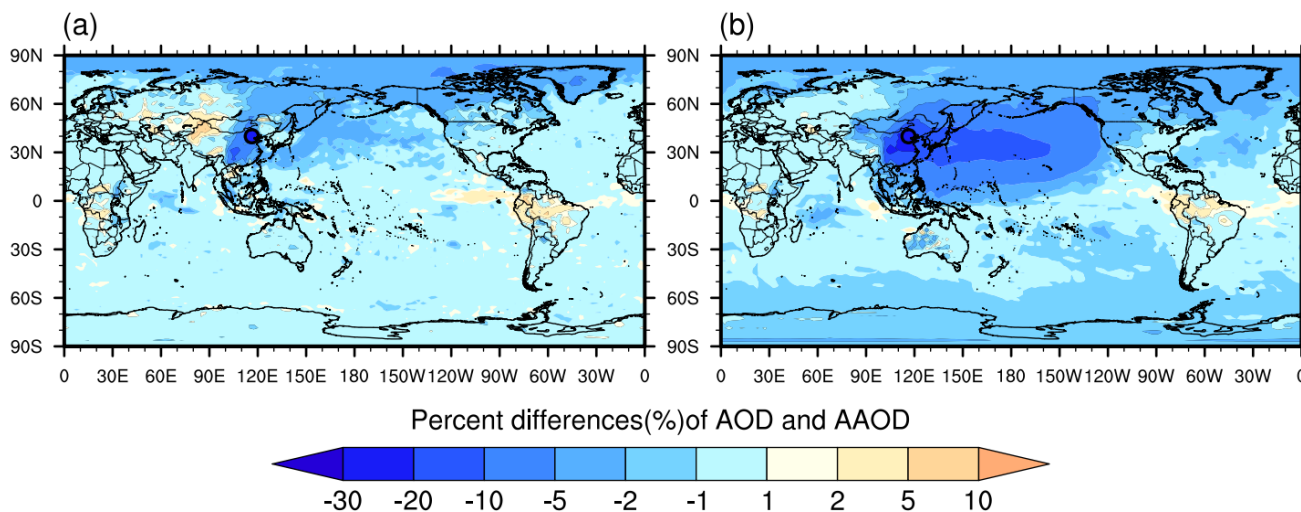
Figure 4. The changes (%) in AOD and AAOD due to variation in anthropogenic emissions in China between 2008 and
205   2016. The observations provided by AERONET are shown in colored dots for comparison with the simulations.

Overall, our model could reproduce the decline in AOD induced by the decrease of sulfate aerosols over China between 2008 and 2016, which have been documented by previous satellite-based studies, and the concurrent decrease of AAOD due to reductions in BC concentrations. Since sulfate and BC play important roles in scattering and absorption effects of aerosols, these changes in AOD and AAOD would impact on the solar radiation budget over China and surrounding areas, as shown in

210 the next section.

3.3 Radiative effects by the change in anthropogenic emissions between 2008 and 2016

Here, we focus on the all-sky aerosol RF at TOA by the inter-annual variation in anthropogenic emissions over China between 2008 and 2016, especially for East China. Both the aerosol shortwave DRF (also termed as RF due to aerosol-radiation interactions) and shortwave + longwave aerosol effects on CRF (including the semi-direct and indirect effects in this study) are considered. As shown in Fig. 5 and Fig. S3, the decrease of sulfate mass burdens due to the substantial reduction in SO_2 emissions induce a positive radiative forcing by diminishing the scattering effects of sulfate aerosols. The mean sulfate DRF is +0.38 W m^{-2} over East China during the study period, with high values of more than 0.6 W m^{-2} in the north part that experiences the most notable reduction in sulfate burdens. As a result of SO_2 emission reductions, nitrate concentrations have increase, and the merged nitrate and ammonium DRF is −0.21 W m^{-2}, though the decrease of particulate ammonium concentrations should yield a positive RF.

The reduction in BC emissions would diminish the absorption effect of BC particles with the decline of the annual mean BC mass burden of 22% over East China between 2008 and 2016. The resultant BC DRF in the Exp16 case is −0.34 W m^{-2} in the region, accounting for 19% of the BC DRE in 2008. Note that in the simulation scenario with BC emission change only (Exp16BC), the BC DRF is −0.29 W m^{-2}, about 15% lower than that in the Exp16 scenario. That is because the concurrent declines in sulfate concentrations and associated water uptake weaken the absorption enhancement of BC-containing particles, and thus further diminish the positive radiative effects of BC. The absorption enhancements by BC coating materials will be overlooked if BC is externally mixed with other aerosols in climate models, which will significantly underestimate the magnitude of the BC DRF for China between 2008 and 2016. Moreover, the treatment of aging processes of BC is another important factor in determining the radiation effects of BC-containing particles. The models with single mixing state for BC-containing particles (without considering the aging processes from fresh BC to thickly-coated BC) could overestimate (underestimate) the BC DRF when BC-containing particles are assumed to be internally mixed (externally mixed) with other components immediately after emissions (Bond et al., 2013; Matsui et al., 2018).

We find that the total aerosol DRF due to all components is −0.18 W m^{-2} over East China between the emission years of 2008 and 2016, with the dominant sources from the reductions in SO_2 and BC emissions (Fig. 6a). Noticeably, the BC and sulfate DRF (−0.34 vs. +0.38 W m^{-2}) are almost counterbalanced by each other. After considering the negative nitrate DRF (−0.21 W m^{-2}) resulting from the SO_2 emission reduction, the net DRF from SO_2 emissions between 2008 and 2016 is +0.17 W m^{-2}. OA and dust aerosols have the mean DRF of −0.06 and +0.003 W m^{-2} and contribute few to the total aerosol DRF during the study period.

On the other hand, we consider aerosol effects on CRF with the combination of semi- and in-direct effects, following Ghan (2013). The variation of BC and SO_2 emissions have distinct impacts on cloud radiative effects. First, as mentioned in Section 3.1, the responses of CCN numbers are negligible to the reduction in BC emissions, but of significant to the reduction in SO_2 emissions with a decrease of 20% for the CCN number concentrations at 0.4% supersaturation. The changes in SO_2 emissions

and associated decline in sulfate would alter in-direct effects by serving as CCN due to its high hygroscopicity (Twomey, 1974; Andreae and Rosenfeld, 2008). By separating the contribution between SO_2 and BC emissions to CRF (the Exp16SO2 and

245   Exp16BC cases), we find that the annual mean CRF is +0.16 W m^{-2} due to the decreased SO_2 emissions in East China between 2008 and 2016, whilst only −0.05 W m^{-2} due to decreased BC emissions. The positive CRF can be explained by the decrease of simulated CCN numbers (Fig. 3), and it is indicative of less solar radiation outgoing back to the space by clouds and therefore potentially warming the atmosphere. By accounting for the interaction between sulfate and BC particles, we find a net aerosol-induced CRF of +0.13 W m^{-2}, and the total RF of that combines aerosol DRF and CRF together is −0.04 W m^{-2} over East

250   China during our study period (Exp08 - Exp16).

While the impacts of SO_2 and BC reductions on RF (DRF + CRF) are very small locally (−0.04 W m^{-2}), there are markedly positive cloud radiative effects mostly within 0.3−0.6 W m^{-2} in the north Pacific region (Fig. 5), with the mean CRF over the north Pacific (marked in Fig. 5f) of +0.16 W m^{-2}, which are associated with the decrease of CCN due to reductions in SO_2 emissions in China (Figs. S3). Since the aerosol DRF in the north Pacific region is negligible, the aerosol effects on cloud

255   dominate the total radiative effects when the anthropogenic emissions in China varied from 2008 to 2016. Our results suggest an important role of SO_2 emissions in China in altering the cloud optical properties in the north Pacific. It should be noted that aerosol effects on cloud radiative properties remain the largest uncertainties in calculating global and regional radiation perturbation by anthropogenic aerosols in current climate models, which should be further constrained by measurements of cloud properties.
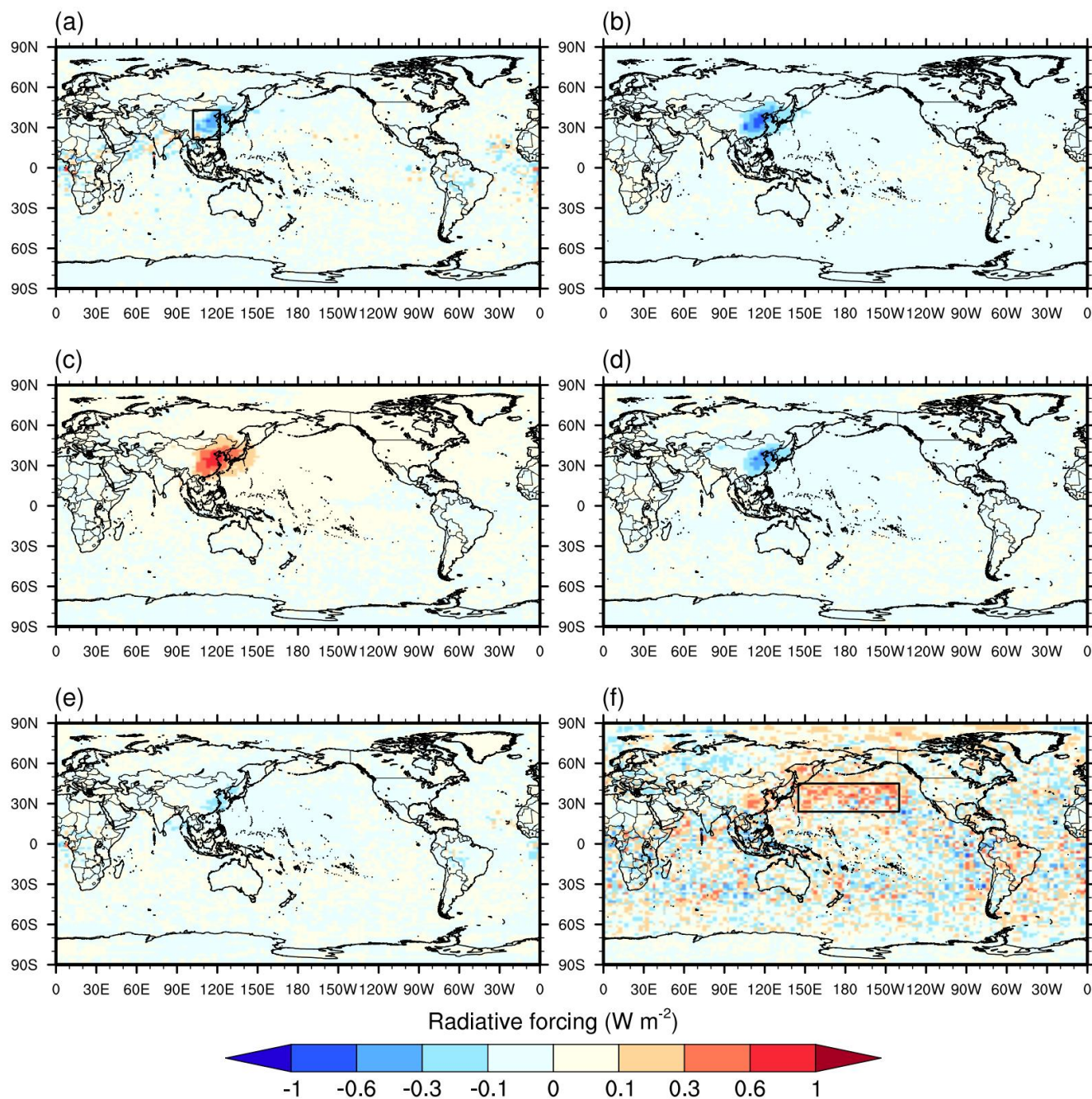
Figure 5. DRF from total aerosols (a), BC (b), sulfate (c), nitrate + ammonium (d), and OA + dust (e), and aerosol-induced CRF (f). Two regions of interest, East China and the north Pacific, are marked in Fig. 5a and 5f with black boxes.
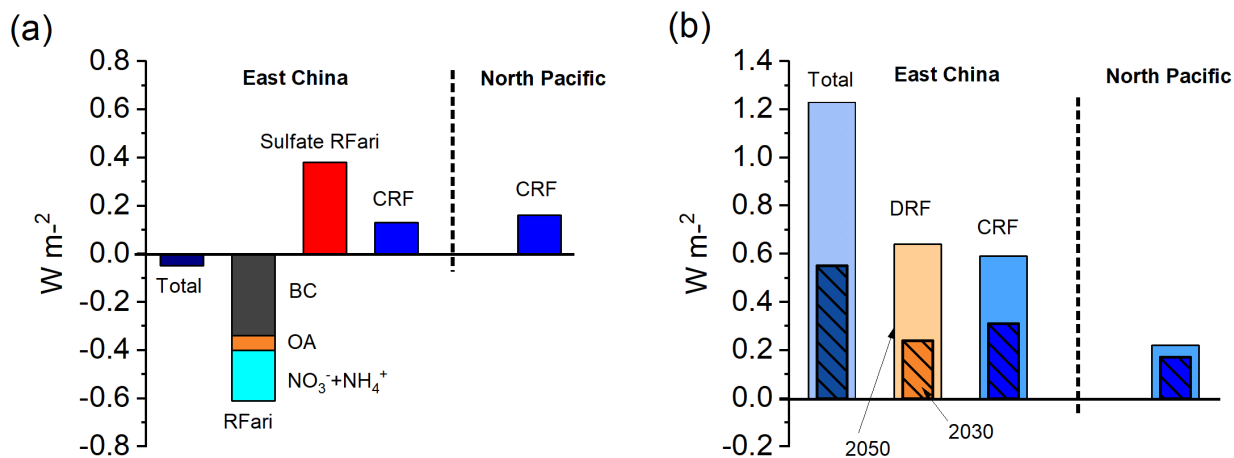
Figure 6. (a) Summary of total RF, RF for major aerosol components due to aerosol-radiation interactions (RFari), and
aerosol effects on clouds (CRF) in East China and the north Pacific due to the changes in anthropogenic emissions between
2008 and 2016; (b) Aerosol DRF and CRF owing to projected anthropogenic emissions for 2030 and 2050 relative to 2016.

In order to understand how aerosol DRF and CRF respond to future emissions, we refer to the projected anthropogenic emission
scenarios in China recently developed by Tong et al. (2020) for 2030 and 2050. For these scenarios, they integrate the shared
socio-economic pathways (SSPs), climate targets of Representative Concentration Pathways (RCPs), and local air pollution
control measures to create dynamic projection of China's emissions in the future decades. Here, among their designed scenarios,
we choose the SSP1-RCP26-BHE (Best Health Effect), which denotes the best-available environmental policies and therefore
the largest reductions of emissions, to predict the upper bound of climate effects from anthropogenic aerosols. We performed
the simulations by using the same meteorological nudging with the historical case for 2008 (Exp08) and scaling anthropogenic
emissions (BC, SO_2, NO_x, OC, VOCs, Primary PM, NH_3, and CO) in China separately from 2016 to 2030 and 2050 in each
grid cell (the scaling factors for each species are shown in Table S1). The projected emissions of greenhouse gases are not
considered and only the aerosol effects on radiation budget are shown here. We find that under the strictest air pollution control
policies, the aerosol DRF are +0.24 W m^{-2} between 2016−2030 and +0.64 W m^{-2} between 2016−2050 over East China. The
total effects with the combination of DRF and CRF reach +0.55 W m^{-2} and +1.23 W m^{-2}, respectively. For this scenario,
although BC emissions keep decreasing in the future, the reductions in scattering aerosols like OA and nitrate induce high
positive RF. For instance, the RF for OA and nitrate due to aerosol-radiation interactions are +0.27 and +0.52 W m^{-2} in our
cases between 2016−2050. In addition, the aerosol effects on clouds in north Pacific are around +0.2 W m^{-2} for the both
2016−2030 and 2016−2050 cases and lower than the CRF in East China.

4. Summary

In this study, we quantify the all-sky aerosol RF for China (especially East China) due to the substantial variation of anthropogenic emissions in the country between 2008 and 2016 using a global climate model. Our simulations demonstrate that the dramatic reductions (−57%) in SO_2 emissions decrease sulfate mass burdens by 35% in East China and 18% in north Pacific, while the burdens of BC are reduced by 25% due to decreased BC emissions (−27%) for this period. It is estimated that the reductions in SO_2 emissions give rise to +0.38 W m^{-2} for sulfate DRF at TOA, −0.21 W m^{-2} for nitrate and ammonium combined DRF, and +0.13 W m^{-2} for aerosol-induced CRF, and meanwhile the BC emission reduction induce a cooling effect of −0.34 W m^{-2} over East China. Since the effects from other aerosol components are negligible for this period, the changes in emissions of SO_2 and BC dominate the aerosol radiative effects between 2008 and 2016. The net RF by the changes in the BC and SO_2 emissions is −0.04 W m^{-2}, implying a small cooling effect. Therefore, we conclude that the radiative forcing by the decline in SO_2 emissions is counteracted by the decreased BC concentrations in China for this period.

While the local radiative forcing is small due to the counteracted effects of SO_2 and BC emissions, there is positive change of about +0.16 W m^{-2} due to aerosol effects on clouds in the north Pacific remote region, primarily contributed by reductions in sulfate particles and their effects on cloud properties via CCN activation. The decrease of sulfate burdens (−18%) in the north Pacific due to the emission control of SO_2 in China results in more than 10% decreases of CCN0.4 in the middle troposphere (700−200 hPa) over the north Pacific, which would reduce the cloud droplet numbers and weaken the cloud albedo, allowing for more solar radiation reaching the earth surface. Therefore, our results highlight the importance of China's SO_2 emissions not only in the contribution to the local radiative forcing, but also in altering the radiation budget in the downwind Pacific regions through the transport of secondary sulfate and associated effects on clouds.

We further predict the aerosol radiative effects using the recently developed China's emission scenario for 2030 and 2050. The results demonstrate that under the strictest environmental policies for China, the total aerosol RF (DRF + CRF) from the projected emission scenarios are +0.55 W m^{-2} between 2016−2030 and +1.23 W m^{-2} between 2016−2050. These effects should be considered by combining with the emission projection of greenhouse gases to better evaluate the responses of climate to future anthropogenic emissions over the regional and global scales.

Appendix A: List of acronyms

AERONET   Aerosol robotic network
AOD   Aerosol optical depth
AAOD   Absorption aerosol optical depth
ATRAS2   Aerosol two-dimensional bin module for formation and aging simulation version 2
BC   Black carbon
BHE   Best health effect
CAM5   Community Atmospheric Model version 5

CCN	Cloud condensation nuclei
CCN0.4	CCN number concentrations at supersaturation of 0.4%
CRF	Cloud radiative forcing
DRE	Direct radiative effect
DRF	Direct radiative forcing
EANET	Acid deposition monitoring network in East Asia
IPCC AR5	The Fifth assessment report of the Intergovernmental Panel on Climate Change
MEIC	Multi-resolution emission inventory for China
MERRA2	Modern-Era retrospective analysis for research and applications version 2
MISR	Multi-angle imaging spectroradiometer
MOZART	Model for ozone and related chemical tracers
N10	particle number concentrations with the diameter larger than 10 nm
NOx	Nitrogen oxides
OC	Organic carbon
RCP	Representative Concentration Pathways
RF	Radiative forcing
RFari	Radiative forcing due to aerosol-radiation interaction
SO$_2$	Sulfur dioxide
SSA	Single scatter albedo
SSP	Shared socio-economic pathways
TOA	Top of the atmosphere

Data availability. EANET observation data is freely available from the online website (https://monitoring.eanet.asia/document/public/index, last access: 10 March 2020). AERONET data for AOD and SSA can be accessed from Goddard Space Flight Center (https://aeronet.gsfc.nasa.gov/new_web/data.html, last access: 20 April 2020). MISR data is available from the Atmospheric Science Data Center at NASA (https://eosweb.larc.nasa.gov/, last access: 20 May 2020). Historical and future anthropogenic emissions for China are provided from the MEIC database (http://www.meicmodel.org/, last access: 15 May 2020).

Author contribution. ML and HM designed the study and wrote the paper. ML performed the simulations and analyzed the results.

Competing interests. The authors declare that they have no conflict of interest.

Acknowledgements. This work was supported by the Ministry of Education, Culture, Sports, Science, and Technology and the Japan Society for the Promotion of Science (MEXT/JSPS) KAKENHI Grant Numbers JP17H04709, JP16H01770, JP19H04253, JP19H05699, and JP19KK0265 and by the MEXT Arctic Challenge for Sustainability (ArCS, Program Grant Number JPMXD1300000000) and ArCS-II projects. This work was also supported by the Environment Research and Technology Development Fund (2–1703 and 2-2003) of the Environmental Restoration and Conservation Agency.

References

Andreae, M. O., and Rosenfeld, D.: Aerosol–cloud–precipitation interactions. Part 1. The nature and sources of cloud-active aerosols, Earth Sci. Rev., 89, 13-41, https://doi.org/10.1016/j.earscirev.2008.03.001, 2008.

Ansari, A. S., and Pandis, S. N.: Response of Inorganic PM to Precursor Concentrations, Environ. Sci. Technol., 32, 2706-2714, 10.1021/es971130j, 1998.

Bond, T. C., Doherty, S. J., Fahey, D. W., Forster, P. M., Berntsen, T., DeAngelo, B. J., Flanner, M. G., Ghan, S., Kärcher, B., Koch, D., Kinne, S., Kondo, Y., Quinn, P. K., Sarofim, M. C., Schultz, M. G., Schulz, M., Venkataraman, C., Zhang, H., Zhang, S., Bellouin, N., Guttikunda, S. K., Hopke, P. K., Jacobson, M. Z., Kaiser, J. W., Klimont, Z., Lohmann, U., Schwarz, J. P., Shindell, D., Storelvmo, T., Warren, S. G., and Zender, C. S.: Bounding the role of black carbon in the climate system: A scientific assessment, J. Geophys. Res.-Atmos, 118, 5380-5552, 10.1002/jgrd.50171, 2013.

Boucher, O., Randall, D., Artaxo, P., Bretherton, C., Feingold, G., Forster, P., Kerminen, V.-M., Kondo, Y., and Liao, H.: Clouds and aerosols. In T. F. Stocker, et al. (Eds.), Climate change 2013: The physical science basis, contribution of Working Group I to the Fifth Assessment Report of the Intergovernmental Panel on Climate Change (pp. 571–658), Cambridge, United Kingdom and New York: Cambridge University Press, 2013.

Charlson, R. J., Schwartz, S. E., Hales, J. M., Cess, R. D., Coakley, J. A., Hansen, J. E., and Hofmann, D. J.: Climate Forcing by Anthropogenic Aerosols, Science, 255, 423, 10.1126/science.255.5043.423, 1992.

Cheng, Y., Zheng, G., Wei, C., Mu, Q., Zheng, B., Wang, Z., Gao, M., Zhang, Q., He, K., Carmichael, G., Pöschl, U., and Su, H.: Reactive nitrogen chemistry in aerosol water as a source of sulfate during haze events in China, Sci. Adv., 2, e1601530, 10.1126/sciadv.1601530, 2016.

Chung, S. H., and Seinfeld, J. H.: Global distribution and climate forcing of carbonaceous aerosols, J. Geophys. Res.-Atmos, 107, AAC 14-11-AAC 14-33, 10.1029/2001JD001397, 2002.

Ghan, S. J.: Technical Note: Estimating aerosol effects on cloud radiative forcing, Atmos. Chem. Phys., 13, 9971-9974, 10.5194/acp-13-9971-2013, 2013.

He, J., Zhang, Y., Glotfelty, T., He, R., Bennartz, R., Rausch, J., and Sartelet, K.: Decadal simulation and comprehensive evaluation of CESM/CAM5.1 with advanced chemistry, aerosol microphysics, and aerosol-cloud interactions, J. Adv. Model. Earth Syst., 7, 110-141, 10.1002/2014ms000360, 2015.

Hoesly, R. M., Smith, S. J., Feng, L., Klimont, Z., Janssens-Maenhout, G., Pitkanen, T., Seibert, J. J., Vu, L., Andres, R. J., Bolt, R. M., Bond, T. C., Dawidowski, L., Kholod, N., Kurokawa, J. I., Li, M., Liu, L., Lu, Z., Moura, M. C. P., O'Rourke, P. R., and Zhang, Q.: Historical (1750–2014) anthropogenic emissions of reactive gases and aerosols from the Community Emissions Data System (CEDS), Geosci. Model Dev., 11, 369-408, 10.5194/gmd-11-369-2018, 2018.

Huang, X., Song, Y., Zhao, C., Li, M., Zhu, T., Zhang, Q., and Zhang, X.: Pathways of sulfate enhancement by natural and anthropogenic mineral aerosols in China, J. Geophys. Res.-Atmos, 119, 14,165-114,179, 10.1002/2014JD022301, 2014.

Huang, X., Song, Y., Zhao, C., Cai, X., Zhang, H., and Zhu, T.: Direct Radiative Effect by Multicomponent Aerosol over China, J. Clim., 28, 3472-3495, 10.1175/jcli-d-14-00365.1, 2015.

Hung, H.-M., and Hoffmann, M. R.: Oxidation of Gas-Phase SO2 on the Surfaces of Acidic Microdroplets: Implications for Sulfate and Sulfate Radical Anion Formation in the Atmospheric Liquid Phase, Environ. Sci. Technol., 49, 13768-13776, 10.1021/acs.est.5b01658, 2015.

Jacobson, M. Z.: Strong radiative heating due to the mixing state of black carbon in atmospheric aerosols, Nature, 409, 695-697, 10.1038/35055518, 2001.

Kanaya, Y., Yamaji, K., Miyakawa, T., Taketani, F., Zhu, C., Choi, Y., Komazaki, Y., Ikeda, K., Kondo, Y., and Klimont, Z.: Rapid reduction of black carbon emissions from China: evidence from 2009-2019 observations on Fukue Island, Japan, Atmos. Chem. Phys. Discuss., 2019, 1-28, 10.5194/acp-2019-1054, 2019.

Koch, D., and Del Genio, A. D.: Black carbon semi-direct effects on cloud cover: review and synthesis, Atmos. Chem. Phys., 10, 7685-7696, 10.5194/acp-10-7685-2010, 2010.

Kulkarni, G., China, S., Liu, S., Nandasiri, M., Sharma, N., Wilson, J., Aiken, A. C., Chand, D., Laskin, A., Mazzoleni, C., Pekour, M., Shilling, J., Shutthanandan, V., Zelenyuk, A., and Zaveri, R. A.: Ice nucleation activity of diesel soot particles at cirrus relevant temperature conditions: Effects of hydration, secondary organics coating, soot morphology, and coagulation, Geophys. Res. Lett., 43, 3580-3588, 10.1002/2016GL068707, 2016.

Li, B., Gasser, T., Ciais, P., Piao, S., Tao, S., Balkanski, Y., Hauglustaine, D., Boisier, J. P., Chen, Z., Huang, M., Li, L. Z., Li, Y., Liu, H., Liu, J., Peng, S., Shen, Z., Sun, Z., Wang, R., Wang, T., Yin, G., Yin, Y., Zeng, H., Zeng, Z., and Zhou, F.: The contribution of China's emissions to global climate forcing, Nature, 531, 357-361, 10.1038/nature17165, 2016.

Li, C., McLinden, C., Fioletov, V., Krotkov, N., Carn, S., Joiner, J., Streets, D., He, H., Ren, X., Li, Z., and Dickerson, R. R.: India Is Overtaking China as the World's Largest Emitter of Anthropogenic Sulfur Dioxide, Sci Rep, 7, 14304, 10.1038/s41598-017-14639-8, 2017.

Li, J.: Pollution Trends in China from 2000 to 2017: A Multi-Sensor View from Space, Remote Sensing, 12, 10.3390/rs12020208, 2020.

Liu, M., Huang, X., Song, Y., Xu, T., Wang, S., Wu, Z., Hu, M., Zhang, L., Zhang, Q., Pan, Y., Liu, X., and Zhu, T.: Rapid SO2 emission reductions significantly increase tropospheric ammonia concentrations over the North China Plain, Atmos. Chem. Phys., 18, 17933-17943, 10.5194/acp-18-17933-2018, 2018.

Liu, M., Song, Y., Xu, T., Xu, Z., Wang, T., Yin, L., Jia, X., and Tang, J.: Trends of Precipitation Acidification and Determining Factors in China During 2006–2015, J. Geophys. Res.-Atmos, 125, e2019JD031301, 10.1029/2019JD031301, 2020.

Liu, X., Easter, R. C., Ghan, S. J., Zaveri, R., Rasch, P., Shi, X., Lamarque, J. F., Gettelman, A., Morrison, H., Vitt, F., Conley, A., Park, S., Neale, R., Hannay, C., Ekman, A. M. L., Hess, P., Mahowald, N., Collins, W., Iacono, M. J., Bretherton, C. S., Flanner, M. G., and Mitchell, D.: Toward a minimal representation of aerosols in climate models: description and evaluation in the Community Atmosphere Model CAM5, Geosci. Model Dev., 5, 709-739, 10.5194/gmd-5-709-2012, 2012.

Matsui, H., Koike, M., Kondo, Y., Fast, J. D., and Takigawa, M.: Development of an aerosol microphysical module: Aerosol Two-dimensional bin module for foRmation and Aging Simulation (ATRAS), Atmos. Chem. Phys., 14, 10315-10331, 10.5194/acp-14-10315-2014, 2014.

Matsui, H.: Black carbon simulations using a size- and mixing-state-resolved three-dimensional model: 2. Aging timescale and its impact over East Asia, J. Geophys. Res.-Atmos, 121, 1808–1821, 10.1002/2015JD023999, 2016.

Matsui, H.: Development of a global aerosol model using a two-dimensional sectional method: 1. Model design, J. Adv. Model. Earth Syst., 9, 1921-1947, 10.1002/2017ms000936, 2017.

Matsui, H., and Mahowald, N.: Development of a global aerosol model using a two-dimensional sectional method: 2. Evaluation and sensitivity simulations, J. Adv. Model. Earth Syst., 9, 1887-1920, 10.1002/2017ms000937, 2017.

Matsui, H., Hamilton, D. S., and Mahowald, N. M.: Black carbon radiative effects highly sensitive to emitted particle size when resolving mixing-state diversity, Nat Commun, 9, 3446, 10.1038/s41467-018-05635-1, 2018.

Morrison, H., and Gettelman, A.: A New Two-Moment Bulk Stratiform Cloud Microphysics Scheme in the Community Atmosphere Model, Version 3 (CAM3). Part I: Description and Numerical Tests, J. Clim., 21, 3642-3659, 10.1175/2008jcli2105.1, 2008.

Myhre, G., Samset, B. H., Schulz, M., Balkanski, Y., Bauer, S., Berntsen, T. K., Bian, H., Bellouin, N., Chin, M., Diehl, T., Easter, R. C., Feichter, J., Ghan, S. J., Hauglustaine, D., Iversen, T., Kinne, S., Kirkevåg, A., Lamarque, J. F., Lin, G., Liu, X., Lund, M. T., Luo, G., Ma, X., van Noije, T., Penner, J. E., Rasch, P. J., Ruiz, A., Seland, Ø., Skeie, R. B., Stier, P., Takemura, T., Tsigaridis, K., Wang, P., Wang, Z., Xu, L., Yu, H., Yu, F., Yoon, J. H., Zhang, K., Zhang, H., and Zhou, C.: Radiative forcing of the direct aerosol effect from AeroCom Phase II simulations, Atmos. Chem. Phys., 13, 1853-1877, 10.5194/acp-13-1853-2013, 2013.

Paulot, F., Paynter, D., Ginoux, P., Naik, V., and Horowitz, L. W.: Changes in the aerosol direct radiative forcing from 2001 to 2015: observational constraints and regional mechanisms, Atmos. Chem. Phys., 18, 13265-13281, 10.5194/acp-18-13265-2018, 2018.

Seinfeld, J. H., and Pandis, S. N.: Atmospheric Chemistry and Physics: From Air Pollution to Climate Change, Third edition ed., John Wiley & Sons, Inc., 2016.

445 Sockol, A., and Small Griswold, J. D.: Intercomparison between CMIP5 model and MODIS satellite-retrieved data of aerosol optical depth, cloud fraction, and cloud-aerosol interactions, Earth Space Sci., 4, 485-505, 10.1002/2017ea000288, 2017.

Stier, P., Seinfeld, J. H., Kinne, S., Feichter, J., and Boucher, O.: Impact of nonabsorbing anthropogenic aerosols on clear-sky atmospheric absorption, J. Geophys. Res.-Atmos, 111, 10.1029/2006JD007147, 2006.

Tong, D., Cheng, J., Liu, Y., Yu, S., Yan, L., Hong, C., Qin, Y., Zhao, H., Zheng, Y., Geng, G., Li, M., Liu, F., Zhang, Y.,
450 Zheng, B., Clarke, L., and Zhang, Q.: Dynamic projection of anthropogenic emissions in China: methodology and 2015-2050 emission pathways under a range of socio-economic, climate policy, and pollution control scenarios, Atmos. Chem. Phys., 20, 5729-5757, 10.5194/acp-20-5729-2020, 2020.

Twomey, S.: Pollution and the planetary albedo, Atmospheric Environment (1967), 8, 1251-1256, https://doi.org/10.1016/0004-6981(74)90004-3, 1974.

455 Wei, C., Wang, M. H., Fu, Q. Y., Dai, C., Huang, R., and Bao, Q.: Temporal Characteristics and Potential Sources of Black Carbon in Megacity Shanghai, China, J. Geophys. Res.-Atmos, 125, 10.1029/2019jd031827, 2020.

Xia, Y., Wu, Y., Huang, R.-J., Xia, X., Tang, J., Wang, M., Li, J., Wang, C., Zhou, C., and Zhang, R.: Variation in black carbon concentration and aerosol optical properties in Beijing: Role of emission control and meteorological transport variability, Chemosphere, 254, 10.1016/j.chemosphere.2020.126849, 2020.

460 Zhang, J., Reid, J. S., Alfaro-Contreras, R., and Xian, P.: Has China been exporting less particulate air pollution over the past decade?, Geophys. Res. Lett., 44, 2941-2948, 10.1002/2017gl072617, 2017.

Zhang, Q., Zheng, Y., Tong, D., Shao, M., Wang, S., Zhang, Y., Xu, X., Wang, J., He, H., Liu, W., Ding, Y., Lei, Y., Li, J., Wang, Z., Zhang, X., Wang, Y., Cheng, J., Liu, Y., Shi, Q., Yan, L., Geng, G., Hong, C., Li, M., Liu, F., Zheng, B., Cao, J., Ding, A., Gao, J., Fu, Q., Huo, J., Liu, B., Liu, Z., Yang, F., He, K., and Hao, J.: Drivers of improved PM2.5 air quality
465 in China from 2013 to 2017, Proceedings of the National Academy of Sciences, 116, 24463, 10.1073/pnas.1907956116, 2019.

Zhao, B., Jiang, J. H., Gu, Y., Diner, D., Worden, J., Liou, K.-N., Su, H., Xing, J., Garay, M., and Huang, L.: Decadal-scale trends in regional aerosol particle properties and their linkage to emission changes, Environ. Res. Lett., 12, 10.1088/1748-9326/aa6cb2, 2017.

470 Zheng, B., Tong, D., Li, M., Liu, F., Hong, C., Geng, G., Li, H., Li, X., Peng, L., Qi, J., Yan, L., Zhang, Y., Zhao, H., Zheng, Y., He, K., and Zhang, Q.: Trends in China's anthropogenic emissions since 2010 as the consequence of clean air actions, Atmos. Chem. Phys., 18, 14095-14111, 10.5194/acp-18-14095-2018, 2018.